Lower Hybrid Drift Waves: Space Observations

Cecilia Norgren,[1,2] Andris Vaivads,[1] Yuri V. Khotyaintsev,[1] and Mats André[1]

[1]*Swedish Institute of Space Physics, Uppsala, Sweden*
[2]*Department of Physics and Astronomy, Uppsala University, Uppsala, Sweden*

Lower hybrid drift waves (LHDWs) are commonly observed at plasma boundaries in space and laboratory, often having the strongest measured electric fields within these regions. We use data from two of the Cluster satellites (C3 and C4) located in Earth's magnetotail and separated by a distance of the order of the electron gyroscale. These conditions allow us, for the first time, to make cross-spacecraft correlations of the LHDWs and to determine the phase velocity and wavelength of the LHDWs. Our results are in good agreement with the theoretical prediction. We show that the electrostatic potential of LHDWs is linearly related to fluctuations in the magnetic field magnitude, which allows us to determine the velocity vector through the relation $\int \delta \mathbf{E} dt \cdot \mathbf{v} = \phi_{\delta B_\parallel}$. The electrostatic potential fluctuations correspond to $\sim 10\%$ of the electron temperature, which suggests that the waves can strongly affect the electron dynamics.

It is characteristic for many plasma environments in the Universe to form extended thin boundaries separating regions of different kind of plasmas. Plasma processes at these boundaries are often of multiscale nature, coupling small electron scales and large magnetohydrodynamics scales, and understanding these boundaries is crucial for many physical phenomena. Such processes are responsible for transport of energy and plasma across the boundaries, plasma energization, and generation of plasma waves. The lower hybrid drift waves (LHDWs) [1,2] are commonly observed at plasma boundaries [3–8], where they often account for one of the strongest electric fields and may result in anomalous diffusion and resistivity [9,10] and electron acceleration [11]. The LHDWs are electron scale waves and therefore detailed experimental characterization of the properties present a challenging task. In the laboratory experiments, dimensions of the electric probes can be of the order of the LHDW wavelength [12]. In contrast, in space plasmas the spacecraft dimensions are much smaller than the LHDW wavelength, which enables detailed *in situ* measurements of the electromagnetic field and plasma properties. On the other hand, to make cross correlation studies of the waves, two spacecraft need to be at electron scale separation, which is seldom the case.

The LHDWs are excited through the lower hybrid drift instability (LHDI) [1] which is a cross field current driven instability with the free energy provided by inhomogeneities in the plasma density and magnetic field. The density gradient length scale, $L_n = (\partial \ln n / \partial x)^{-1}$, necessary to excite the LHDI can be of the order of several ion gyroradii. L_n is related to the ion diamagnetic drift through $L_n/\rho_i = v_{\text{th},i}/2v_{Di}$, where $\rho_i = v_{\text{th},i}/\Omega_i$ is the ion gyroradius, $v_{\text{th},i} = \sqrt{2T_i/m_i}$ is the ion thermal velocity, and $v_{Di} = T_i/eBL_n$ is the ion diamagnetic drift velocity, assuming the temperature to be approximately constant. The nature of the LHDI is twofold, in the presence of a weak gradient case, $v_{Di} < v_{\text{th},i}$, it is a kinetic instability where a drift wave resonates with drifting ions. In the strong gradient case, $v_{Di} > v_{\text{th},i}$, it is a fluid instability where a drift wave couples to a lower hybrid wave [1]. The maximum growth rate occurs in the strong drift regime, with the following properties [13]:

$$\omega_r \sim \omega_{\text{LH}}, \quad \gamma \lesssim \omega_{\text{LH}}, \quad k_\perp \rho_e \sim 1, \quad \mathbf{k} \cdot \mathbf{B} = 0, \qquad (1)$$

where $\omega = \omega_r + i\gamma$ and k are the complex frequency and wave number of the mode, $\rho_e = v_{\text{th},e}/\Omega_e$ is the electron gyroradius, and $\omega_{\text{LH}} = \omega_{pi}(1 + \omega_{pe}/\Omega_e)^{-1/2}$ is the lower hybrid frequency. At these frequencies and wavelengths, the electrons are strongly magnetized while the ions are unmagnetized, a fact that lets the ions move across the magnetic field and interact resonantly with the waves. As the wave vector gains a parallel component, $k_\parallel$, the electrons can be accelerated along the field lines due to Landau resonance, which has a strong stabilizing effect [11]. The LHDI is stabilized by finite plasma β [4,13]. When $\beta \gtrsim 1$, it is instead a longer wavelength magnetic mode, $k_\perp \sqrt{\rho_e \rho_i} \sim 1$, which becomes dominant [14]. Some of the fundamental properties of the fastest growing shorter wavelength mode, $k_\perp \rho_e \sim 1$, such as phase velocity and wavelength have been estimated [3,15], but never measured directly. In this Letter, we report such measurements for the first time.

From July to November, 2007, two of the Cluster spacecraft [16], C3 and C4, were down to a separation distance of as little as 40 km. We present data from August 31, 2007, when Cluster crosses a plasma boundary in Earth's magnetotail, at $[-14 \ -4 \ 2]R_E$ in geocentric solar magnetospheric (GSM) coordinates. This event fulfilled the following conditions: (1) presence of a clear plasma boundary with gradients in density and magnetic field as well as strong electric fields, (2) a high value of the local electron gyroradius, allowing the two spacecraft to observe

the same electron scale structure, and (3) the spacecraft operates in burst mode, allowing the highest possible time resolution measurement of both the electric and magnetic field. Figure 1 shows an overview of the event as seen by C4 (C3 observes the same large scale picture and is not shown here). At 10:19 UT (universal time) the spacecraft cross a sharp plasma boundary seen as a sharp decrease in the magnetic field strength [Fig. 1(a)], corresponding to a narrow current layer, with a simultaneous change in both the electron and ion populations [Figs. 1(b) and 1(c)], as more energetic particles appear, and a sharp increase in the plasma density and plasma beta [Fig. 1(d)]. At this plasma boundary, we observed high amplitude electric fields [Fig. 1(e)]. Spectral analysis show presence of oscillations in the lower hybrid frequency range in both the electric and magnetic field [Figs. 1(f) and 1(g)]. The area with high amplitude electric field consists of several wave packets,
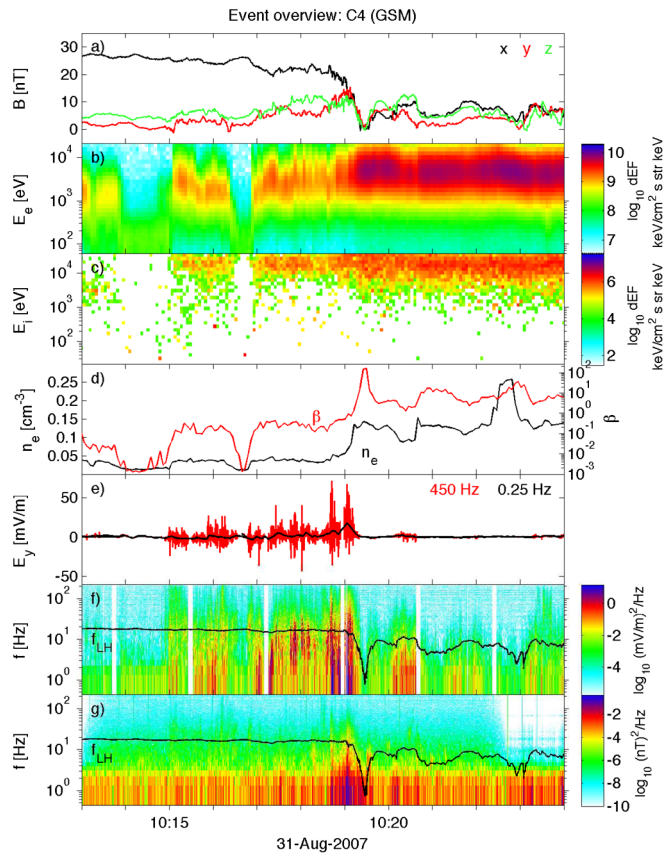

FIG. 1 (color online). Overview of the boundary layer crossing. (a) The magnetic field. (b) The electron energy flux as well as (c) the ion energy flux. (d) The electron density and plasma beta. (e) One component of the electric field, both full resolution (red) and a four second average (black). (f) The electric field power spectrum and (g) the magnetic field power spectrum. The lower hybrid frequency is plotted as a black line in (f) and (g). We study in detail the region at 10:19 UT where the largest amplitude electric field variations in the lower hybrid frequency range are observed.

possibly due to the spacecraft passing in and out of the current sheet. We study one of them in detail.

Because the LHDWs propagate in a current sheet nearly perpendicular to the ambient magnetic field, we use a magnetic field aligned coordinate system. The unit vectors are given by $\hat{\mathbf{z}} = \mathbf{B}/|\mathbf{B}|$, $\hat{\mathbf{y}} = \hat{\mathbf{z}} \times (\hat{\mathbf{n}} \times \hat{\mathbf{z}})$, and $\hat{\mathbf{x}} = \hat{\mathbf{y}} \times \hat{\mathbf{z}}$, where $\mathbf{B}$ is the average magnetic field from the short time interval during which we observe the individual wave packets, and $\hat{\mathbf{n}}$ is the current layer normal which we obtain by performing a minimum variance analysis on the magnetic field during a longer interval from 10:18:36 to 10:19:28 UT. The results for both C3 and C4 were practically identical, with the eigenvalue ratio $L_2/L_3 = 10$. The expected LHDW propagation direction, $\hat{\mathbf{x}}$, is given by the third direction, perpendicular to both $\mathbf{B}$ and $\hat{\mathbf{n}}$. The resulting configuration of the spacecraft in this system is shown in Fig. 2(a), which also shows the ion drift obtained from the Cluster Ion Spectrometry experiment, and the average $\mathbf{E} \times \mathbf{B}$ drift. As the $\mathbf{E} \times \mathbf{B}$ drift is close to the wave propagation direction, its small $\hat{\mathbf{n}}$ component cannot be reliably used to estimate the motion of the current layer. The separation between C3 and C4 in the $\hat{\mathbf{x}}$ direction is ~9 km, which is smaller than the theoretically expected wavelength of the LHDW, $\lambda_{LH} \approx 2\pi\rho_e \approx 55$ km. This provides excellent conditions to observe the same LHDW packet on both C3 and C4.

We use simultaneous observations of the electric field on C3 and C4 to perform cross correlation measurements of the LHDWs. Figures 2(b) and 2(c) shows electric field observations during 10:19:05.50–10:19:05.90 UT. Two components are shown: the electric field along the propagation direction of the wave, E_x [Fig. 2(b)], and in the normal direction, E_y [Fig. 2(c)]. As the Electric Field and Wave instrument aboard Cluster only measures the electric field in the spacecraft spin plane, we first reconstruct the nonmeasured component of $\mathbf{E}$ assuming $\mathbf{E} \cdot \mathbf{B} = 0$ ($\mathbf{B}$ is at ~60° with respect to the spacecraft spin plane), and then make the transformation to the field aligned coordinate system. C3 and C4 observe very similar time series in the x component, that is the expected propagation direction of the wave. To obtain the phase velocity of the waves, we find the time shift that gives the highest correlation between the two time series. This analysis is performed on both components and we find the highest correlation for E_x (correlation coefficient = 0.74 as opposed to 0.53 for E_y) which results in a time shift of $\Delta t = 6.4$ ms [the shifted electric field from C4 is shown in Figs. 2(b) and 2(c) as a blue dashed line] and a phase velocity of 1400 (±300) km/s. We see that the phase velocity of the wave is comparable to the ion drift velocity as measured by the Cluster Ion Spectrometry experiment. This is expected from theory because the ions must be in resonance with the wave in order to drive the wave growth. By knowing the phase velocity of the wave we can associate a length scale with our observations that is shown on
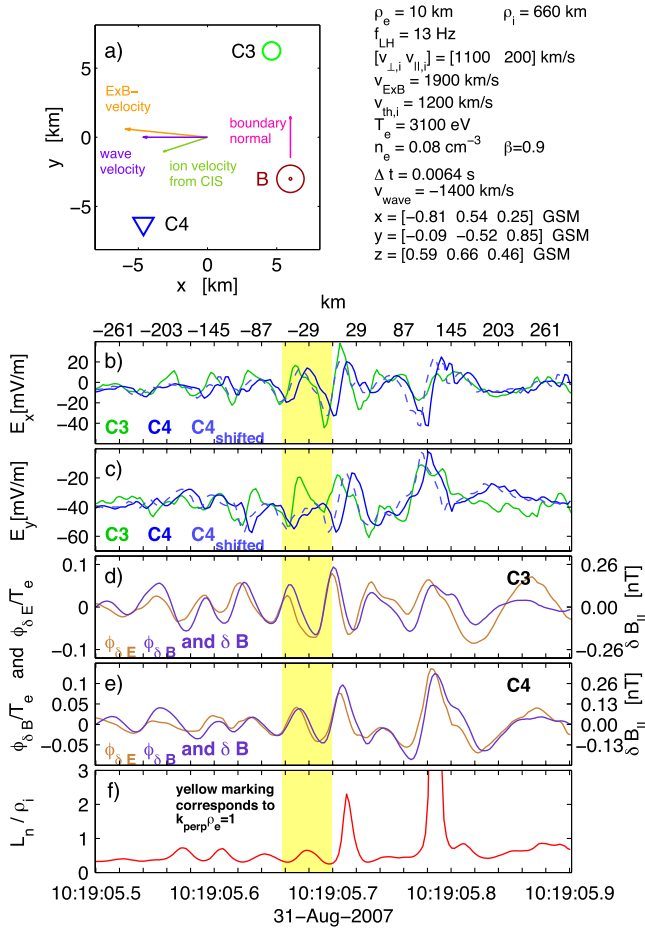
FIG. 2 (color online).   A lower hybrid drift wave packet. (a) The spacecraft configuration and particle flows in the field aligned coordinate system. The electric field in (b) the propagation direction of the wave and (c) normal direction of the current sheet. Solid lines show observation by C3 (green, lighter) and C4 (blue, darker), respectively. The time shifted field of C4 is shown as a dashed line and results in $\nu = 1400$ km/s and $\lambda \approx 60$ km. The shaded yellow area marks $k_\perp \rho_e = 1$. (d),(e) The electrostatic potential, normalized to the electron temperature, obtained from $\delta E_\perp$ (orange, lighter) and $\delta B_\parallel$ (purple, darker), as measured by C3 and C4, respectively. The right-hand scale shows the amplitude of $\delta B_\parallel$. (f) The gradient length scale normalized to the ion gyroradius.

top of Fig. 2(b). The shaded yellow marking corresponds to the wavelength of the maximum growing mode according to theory, which for this time interval is $\lambda_{LH} = 55$ km. The observed wavelength is ~60 km which is in good agreement with the theoretical prediction.

An important parameter for the LHDI is the gradient length scale, L_n. We estimate L_n measuring the difference in the magnetic field between C3 and C4, and assuming balance of total pressure [Fig. 2(f)]. For the largest part of the time interval, L_n/ρ_i is below 1, indicating that we are in between the strong and the weak drift regime and that the density gradient is sharp enough to sustain the LHDI. If we assume that the ion velocity is mainly given by the diamagnetic drift, we get a ratio of $L_n/\rho_i = v_{th,i}/2v_{Di} \approx 0.5$

[see Fig. 2(a)], which is consistent with what we see during the larger part of the time interval in Fig. 2(f). While the presence of a temperature gradient is possible, it is hard to make reliable cross-spacecraft estimates of particle data due to the low time resolution of the particle instruments (4 s) compared to the wave period.

Using the phase velocity of the wave, **v**, we can integrate the wave electric field (which is obtained by high pass filtering the total electric field at half of the lower hybrid frequency in order to single out the largest contribution from the waves) to obtain the electrostatic potential associated with the wave: $\phi_{\delta E} = \int \delta \mathbf{E} dt \cdot \mathbf{v}$. The resulting potential, normalized to the electron temperature, is shown in Figs. 2(d) and 2(e), orange (lighter) line. The potential varies from -100 to 300 V at its maximum which corresponds to potential fluctuations of ~10% of the electron temperature, suggesting that the electrons could be effectively scattered by the wave. This is in line with laboratory experiments that estimate the normalized wave potential fluctuations to be on the order of $\lesssim 10\%$ [5].

We note in Figs. 2(d) and 2(e) a strong correlation between $\phi_{\delta E_\perp}$ and $\delta B_\parallel$. This can be explained if we remember that the ions can be considered unmagnetized, so that the electrons will carry a current through the $\delta \mathbf{E} \times \mathbf{B}_0$ drift. This perpendicular current will, according to Ampère's law and because $k_\parallel \ll k_\perp$, correspond predominantly to changes in the magnetic field, $\delta B_\parallel$, along the direction of the ambient magnetic field. This assumption is supported by a minimum variance analysis, where we also observe small perpendicular components δB_x and δB_y, making it impossible to deduce the propagation direction from $\nabla \cdot \delta \mathbf{B} = 0$. Based on these assumptions we can derive a linear relation between $\delta B_\parallel$ and the expected electrostatic potential of the wave $\phi_{\delta B_\parallel}$:

$$\phi_{\delta B_\parallel} = \frac{B_0}{n_e e \mu_0} \delta B_\parallel, \qquad (2)$$

which is shown by a purple (darker) line in Figs. 2(d) and 2(e) with the magnitude of the wave magnetic field shown on the right-hand scale. $\phi_{\delta B_\parallel}$ and $\phi_{\delta E_\perp}$ are in excellent agreement. The agreement between $\phi_{\delta B_\parallel}$ and $\phi_{\delta E_\perp}$ confirms two things: first, the reasoning that led to Eq. (2) is correct, and second, we have indeed a good estimate of the propagation direction and velocity. Relationship (2) could be seen as a first order approximation of the electromagnetic component of the LHDWs. As the density increases further into the current sheet, so will the $\delta \mathbf{E} \times \mathbf{B}_0$ current and the magnetic perturbation, possibly being one of the reasons why the LHDWs tend to become more electromagnetic than electrostatic in this region [17]. A parallel magnetic component has been investigated before in space [3] and is also indicated in computer simulations [14], where one can see that the maxima and minima of $\phi_{\delta B_\parallel}$ and $\delta B_\parallel$ coincide over the thickness of the current layer, and also that their relative
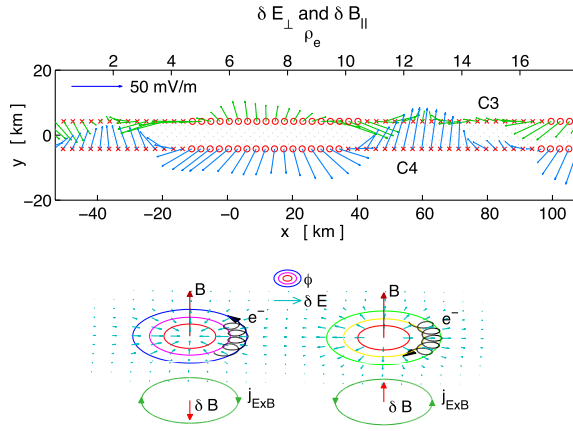
FIG. 3 (color online).　(Top) Perpendicular wave electric field and (anti)parallel ($\times$ / $\bigcirc$) wave magnetic field for each time step. Note that this is not the same wave packet that is shown in Fig. 2 but is part of a wave packet observed during the time 10:19:04.70–10:19:04.90 UT. (Bottom) A schematic image explaining the repetitive pattern seen in the top image.

amplitude varies. The relation between $\phi_{\delta B_\parallel}$ and $\delta B_\parallel$ allows us to determine the wave properties from single spacecraft measurements. Because the shape of the potential is dependent on the propagation direction, and the amplitude is dependent on the propagation velocity, we can deduce the wavelength and the phase velocity of the wave by finding the propagation direction and velocity that gives the best match between $\phi_{\delta B_\parallel}$ and $\phi_{\delta E_\perp}$, i.e., find **v** so that $\int \delta \mathbf{E} dt \cdot \mathbf{v} = \phi_{\delta B_\parallel}$. If we apply this to the case presented in Fig. 2, we find the velocity $\mathbf{v} \approx 1400 \times [0.76 \ -0.64 \ -0.05]$ km/s (GSM), which is at an angle of $\sim 10°$ with the propagation direction, $-\hat{\mathbf{x}}$, which was found by means of minimum variance analysis, suggesting a small local variation of the direction of the current layer. Using this method, we will be able to examine the LHDWs in a wider parameter space, further exploring the wave properties.

In order to illustrate the potential structure of the waves, we plot in Fig. 3 (top), for each time step, $\delta \mathbf{E}_\perp$, and the sign of $\delta B_\parallel$, observed by C3 and C4. This is done for another wave packet than in Fig. 2, that has a longer wavelength, $\lambda \approx 90$ km, and better illustrates the clear potential structure of the waves. It can be seen that $\delta \mathbf{E}_\perp$ forms vortex structures, and that C3 and C4 are alternatively on the same side or on the opposite side of these structures as they propagate by. There is also a clear correlation between $\delta B_\parallel$ and $\delta \mathbf{E}_\perp$. In the locations where $\delta \mathbf{E}_\perp$ converges, $\delta \mathbf{B}_\parallel$ is antiparallel to $\mathbf{B}_0$, and where $\delta \mathbf{E}_\perp$ diverges, $\delta \mathbf{B}_\parallel$ is parallel to $\mathbf{B}_0$, which is illustrated in Fig. 3 (bottom).

In summary, using Cluster data from 2007 when two of the spacecraft (C3 and C4) were ~ 40 km apart in Earth's magnetotail, and as close as ~ 10 km transverse to the magnetic field, we have made detailed studies of the

LHDWs. Apart from the event presented here, we have performed similar analysis for 10 other closely located events on the same day and found similar wave properties, $k\rho_e \sim 0.5 - 1$. By estimating the propagation direction of the wave and matching the time series of the two spacecraft, we are for the first time able to directly measure the phase velocity of the LHDW, which was on the order of 1400 km/s and comparable to the ion velocity. Using this velocity we could deduce, for the first time, the wavelength (~ 60 km) which corresponds well with the theoretical wavelength of the maximum growing mode ($\lambda_{\mathrm{LH}} = 55$ km). By estimating the gradient length scale across the current layer, we could verify that the theoretical existence conditions for the LHDI were indeed met. We integrated the electric field and found electrostatic potential fluctuations which corresponded to about 10% of the electron temperature, indicating efficient interaction between electrons and LHDWs.

[1] N. A. Krall and P. C. Liewer, Phys. Rev. A **4,** 2094 (1971).
[2] J. D. Huba, N. T. Gladd, and K. Papadopoulos, Geophys. Res. Lett. **4,** 125 (1977).
[3] J. D. Huba, N. T. Gladd, and K. Papadopoulos, J. Geophys. Res. **83,** 5217 (1978).
[4] S. D. Bale, F. S. Mozer, and T. Phan, Geophys. Res. Lett. **29,** 2180 (2002).
[5] T. A. Carter, M. Yamada, H. Ji, R. M. Kulsrud, and F. Trintchouk, Phys. Plasmas **9,** 3272 (2002).
[6] A. Vaivads, M. André, S. C. Buchert, J.-E. Wahlund, A. N. Fazakerley, and N. Cornilleau-Wehrlin, Geophys. Res. Lett. **31,** L03804 (2004).
[7] M. Zhou et al., J. Geophys. Res. **114,** A02216 (2009).
[8] Yu. V. Khotyaintsev, C. M. Cully, A. Vaivads, M. André, and C. J. Owen, Phys. Rev. Lett. **106,** 165001 (2011).
[9] R. C. Davidson and N. T. Gladd, Phys. Fluids **18,** 1327 (1975).
[10] I. Silin, J. Büchner, and A. Vaivads, Phys. Plasmas **12,** 062902 (2005).
[11] I. H. Cairns and B. F. McMillan, Phys. Plasmas **12,** 102110 (2005).
[12] W. Fox, M. Porkolab, J. Egedal, N. Katz, and A. Le, Phys. Plasmas **17,** 072303 (2010).
[13] R. C. Davidson, N. T. Gladd, C. S. Wu, and J. D. Huba, Phys. Fluids **20,** 301 (1977).
[14] W. Daughton., Phys. Plasmas **10,** 3103 (2003).
[15] C. A. Cattell and F. S. Mozer, Geophys. Res. Lett. **13,** 221 (1986).
[16] C. P. Escoubet, M. Fehringer, and M. Goldstein, Ann. Geophys. **19,** 1197 (2001).
[17] I. Shinohara, T. Nagai, M. Fujimoto, T. Terasawa, T. Mukai, K. Tsuruda, and T. Yamamoto, J. Geophys. Res. **103,** 20 365 (1998).